Quantum Hall induced currents and the magnetoresistance of a quantum point contact

2011 New J. Phys. 13 123020

(http://iopscience.iop.org/1367-2630/13/12/123020)

New Journal of Physics
The open-access journal for physics

Quantum Hall induced currents and the magnetoresistance of a quantum point contact

M J Smith[1], C D H Williams[1], A Shytov[1], A Usher[1,3], A S Sachrajda[2], A Kam[2] and Z R Wasilewski[2]

[1] School of Physics, University of Exeter, Stocker Road, Exeter EX4 4QL, UK
[2] Institute for Microstructural Sciences, National Research Council of Canada, Ottawa, ON, K1A 0R6, Canada
E-mail: a.usher@exeter.ac.uk

New Journal of Physics **13** (2011) 123020 (12pp)
Received 13 October 2011
Published 13 December 2011
Online at http://www.njp.org/
doi:10.1088/1367-2630/13/12/123020

Abstract. We report an investigation of quantum Hall induced currents by simultaneous measurements of their magnetic moment and their effect on the conductance of a quantum point contact (QPC). Correlation of features in the noise of the induced currents, caused by the breakdown of the quantum Hall effect, for the two types of measurements provides conclusive proof of the common origin of the two effects. Common features in the magnetic moment and QPC resistance at Landau-level filling factors $\nu = 1, 2$ and 4 and their similar temperature and nonlinear sweep-rate dependences support this conclusion. In contrast, there is a distinct difference in the way the induced currents decay with time when the sweeping field halts at integer filling factor as detected by the two types of measurement. We attribute this difference to the fact that, while both effects are sensitive to the magnitude of the induced current, the QPC resistance is also sensitive to the proximity of the current to the QPC split gate, and we develop a model that describes semi-quantitatively the effects we observe. Although it is clearly demonstrated that induced currents affect the electrostatics of a QPC, the reverse effect, the QPC influencing the induced current, is not observed.

[3] Author to whom any correspondence should be addressed.

Contents

1. Introduction

The occurrence of long-lived induced currents when a two-dimensional electron system (2DES) is in the quantum Hall effect (QHE) regime demonstrates the extraordinarily low dissipation accompanying the effect (for a review, see Usher and Elliott [1]). First observed through the magnetization they produce [2–4], induced currents are expected to be present in conventional quantum Hall measurements, but are not detectable in such experiments despite often being orders of magnitude larger than the currents injected into the 2DES through the electrical contacts. Klaffs *et al* [5] suggested an explanation for the isolation of induced currents from injected currents based on the picture of Chklovskii *et al* [6]: in high magnetic fields the edge of the 2DES separates into compressible and incompressible strips; at integer Landau-level filling factors, ν, the innermost incompressible strip spreads into the bulk [7] and the induced current then flows in the compressible strip at the outside edge of the *innermost* incompressible strip. Injected currents flow in the *outer* strips.

We recently discovered that induced currents *can* influence conventional transport measurements in electrostatically defined nanostructures such as quantum point contacts (QPCs) and quantum dots [8]. Features were observed in the conductance of a QPC and in the Coulomb blockade spectrum of a quantum dot which were hysteretic with respect to the magnetic-field sweep direction. In the same work, separate experiments measuring the magnetic moment associated with the QHE induced currents showed that they were present in a separate 2DES formed from the same wafer, grown by molecular beam epitaxy, from which the nanostructures were fabricated. The filling factor, temperature and sweep-rate dependences of the induced currents in the heterojunction correlated with the hysteretic behaviour observed within the nanostructures, suggesting that a common origin was possible. However, since these measurements were carried out in separate experiments and on different devices, and correlations were only seen at two Landau-level filling factors, the correlations could have been coincidental. In this paper, we report the first *simultaneous* measurements of induced currents in the same device, from their magnetic moments and their effects on QPC conductance. Common features in the noise accompanying the induced currents in the QHE breakdown regime, as well as correlations in the temperature and sweep-rate dependences at $\nu = 1, 2$ and 4, prove

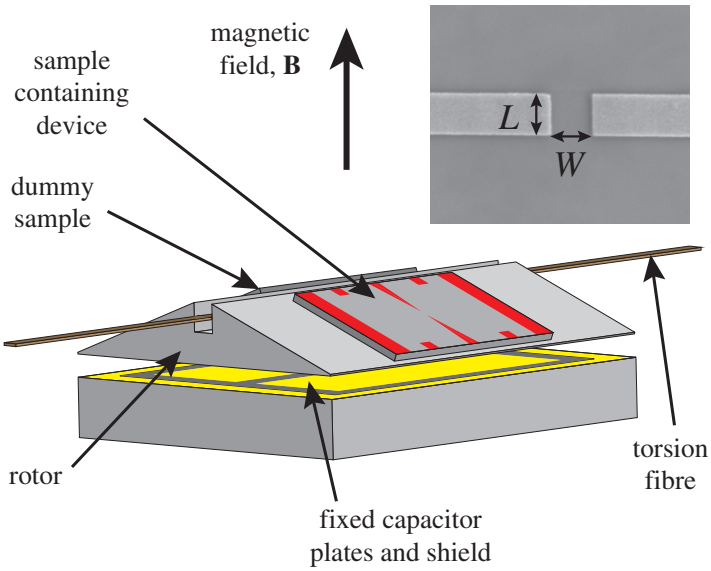

Figure 1. Schematic diagram of the QPC device mounted on the torsion-balance magnetometer. The magnetic moment **m** caused by the induced currents circulating in the 2DES 'leads' of the device produces a torque, $\mathbf{m} \times \mathbf{B}$. This is detected as an imbalance of the differential capacitor formed by an electrode on the underside of the rotor and the two fixed capacitor plates shown. Simultaneously, the QPC conductance is measured; electrical connections to the device are not shown on the diagram, for clarity. The inset is a scanning electron microscope image of the QPC split gate, $W = 509\,\text{nm}$ and $L = 503\,\text{nm}$.

conclusively the common origin of the two effects. The measurements also demonstrate that the QPC resistance is sensitive not only to the magnitude of the induced current but also to its distance from the QPC split gate. We develop a model based on the work of Fertig and Halperin [9], which helps us to explain some of the differences between the behaviour of the QPC resistance and that of the magnetic moment.

2. Experimental details

The device was fabricated at the Institute for Microstructural Sciences[4], from a GaAs–(Al,Ga)As heterojunction, forming a 2DES of dimensions $4.0\,\text{mm} \times 4.5\,\text{mm}$ with a metallic split gate defined on the surface, approximately 110 nm above the 2DES. The mobility of the 2DES was $103\,\text{m}^2\,(\text{V s})^{-1}$ at 4 K and its number density was $2.01 \times 10^{15}\,\text{m}^{-2}$. The split gate was centred over the 2DES. The lithographic dimensions of the gate are given in figure 1. The QPC was defined electrostatically by the application of a negative bias, with respect to the 2DES, to both sides of the split gate. Gold ohmic contact pads on the QPC were connected to insulated copper twisted pairs (25 μm diameter with approximately three twists per millimetre) with colloidal silver paint[5]. The device was mounted on the rotor of

[4] Institute for Microstructural Sciences, NRC-CNRC Canada, sample designation 'AK47'.

[5] Silver paint: Silver in Methyl Isobutyl Ketone. Manufacturer brand: Acheson Electrodag 1415M. Distributed by Agar Scientific (product number G3648), batch no. 0334. Agar Scientific, Essex, UK.

a torsion-balance magnetometer (figure 1), details of which are given elsewhere [10]. The normal to the 2DES was tilted at an angle of 20° to the applied magnetic field. The wires from the device were arranged to minimize mechanical perturbation of the magnetometer.

In order to reduce noise, predominantly manifest as telegraph noise [11], the sample was cooled from room temperature with a gate voltage of +0.26 V applied. This removed free charge from the gate region while it was still mobile. A standard four-terminal measurement with a low-frequency (17.3 Hz) lock-in detector was used to determine the QPC resistance, with an excitation current of 10 nA. Once cold, the gate voltage was set to a negative value such that conduction through the QPC was below $2e^2/h$ and hence the mechanism for conduction was quantum tunnelling. In this state, the QPC was very sensitive to changes in its local electrostatic environment. With this arrangement, *simultaneous* measurements were carried out of the magnetic moment of the induced current in the regions of 2DES either side of the QPC, and of the conduction through the QPC.

The magnetometer occupied the mixing chamber of a dilution refrigerator and measurements were taken between 39 mK and 1.6 K. The magnetic field was produced by a 19 T solenoid, driven by an Oxford Instruments IPS 120-20 digital power supply.

3. Results and discussion

3.1. Simultaneous measurements of magnetic moment and quantum point contact resistance

Figure 2 shows the results of the simultaneous measurement of the magnetic moment and the QPC resistance. Evidence of induced currents (features that reverse with the magnetic-field sweep direction) are seen at Landau-level filling factors $\nu = 1, 2$ and, for the first time, 4 in both the magnetic moment and the QPC resistance data. The smaller features in the magnetic moment at $\nu = 3$, 6, 8 and 10 are primarily caused by capacitive coupling between the 2DES and the capacitor plates (the shield referred in to figure 1 was designed to minimize this coupling), but on close inspection also show small hysteretic effects.

The relative sizes of the features $\nu = 1$, 2 and 4 for the magnetic moment are approximately 1.7 : 1.7 : 1, while for the QPC magnetoresistance features they are 46 : 4.3 : 1.

In order to understand this difference, we follow the arguments of Fertig and Halperin [9] and approximate the potential of the QPC as a quadratic saddle point. In the direction parallel to the flow of current through the QPC the parabolic potential is given by $V_x = -m\omega_x^2 x^2/2$, and in the perpendicular direction it is given by $V_y = m\omega_y^2 y^2/2$. The resistance of the QPC is then given by

$$R(B) = \frac{h}{e^2} \exp\left(-\pi \frac{\Delta E}{E_1(B)}\right), \tag{1}$$

where ΔE is the Fermi energy of the 2D electrons relative to the saddle-point energy, $\Delta E = E_F$, and $E_1(B)$ is a parameter describing the effective potential of the QPC in terms of V_x, V_y and $\omega_c = eB/m^*$ (the cyclotron frequency), and is given by equation (1.4) of Fertig and Halperin [9]. To estimate these frequencies, we first note that at the pinch-off point the contact should have an effective width of the order of the Fermi wavelength, which is about 50 nm. Since the length of the contact, $L = 503$ nm, is significantly larger, one can conclude that the curvature in the current direction is significantly lower, i.e. $\omega_x \ll \omega_y$. Under such conditions, equation (1.4) of

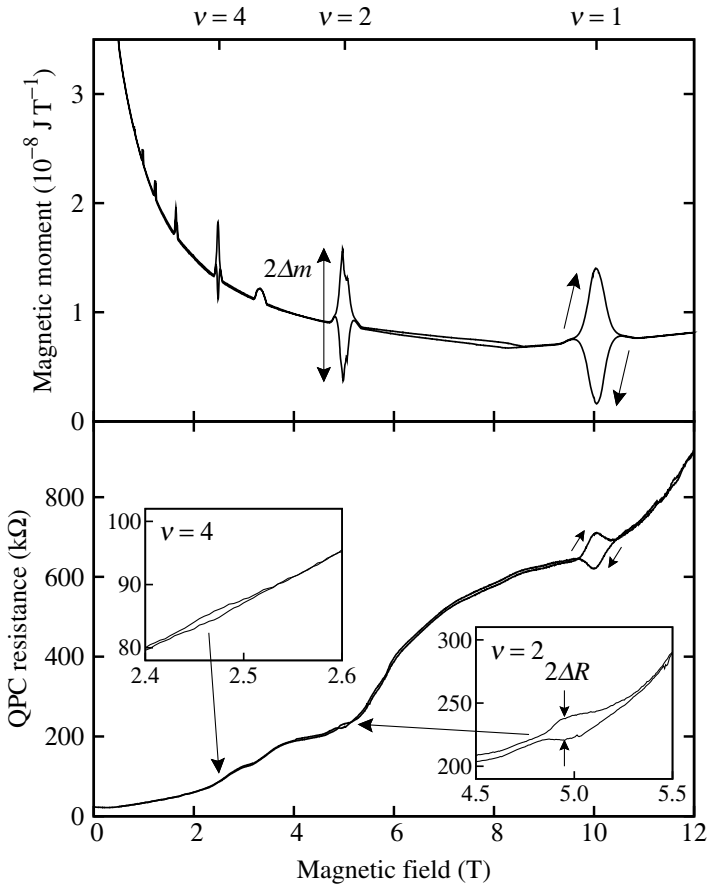

Figure 2. Simultaneous measurement of magnetic moment (upper trace) and QPC resistance (lower trace) at 300 mK. The magnetic-field sweep rate was 1.6 mT s^{-1}. Arrows indicate the magnetic-field sweep directions. The two insets show the detail of the hysteretic resistance at $\nu = 2$ and $\nu = 4$. The quantities Δm and ΔR marked on the figures are the quantities plotted for various filling factors in figures 5–7.

Fertig and Halperin [9] simplifies to

$$E_1(B) = \frac{\hbar\omega_x\omega_y}{2\sqrt{\omega_y^2 + \omega_c^2}}. \tag{2}$$

At $B = 0$, $E_1 = \hbar\omega_x/2$; at large B, $E_1 = \hbar\omega_x\omega_y/2\omega_c$. The sensitivity of the QPC to local electric fields, such as the Hall field set up by the induced currents, is inversely proportional to $E_1(B)$. To estimate the magnetic field dependence of the QPC sensitivity, we have performed a numerical simulation based on classical electrostatics and the Thomas–Fermi screening model. The electrical potential is calculated from the charge distributions of the 2DES and on the gate, and these distributions are adjusted until they give a constant potential on the gate that satisfies the Thomas–Fermi relation on the 2DES. (The density on the 2DES is set to zero when the electrical potential exceeds the Fermi energy.) This approach gives $\omega_x = 8 \times 10^{11}$ s^{-1} and $\omega_y = 9 \times 10^{12}$ s^{-1}. The resulting QPC sensitivity is shown in figure 3. One can see that the sensitivity is independent of B at low fields, $B < 2$ T, and becomes linear in B at high fields.

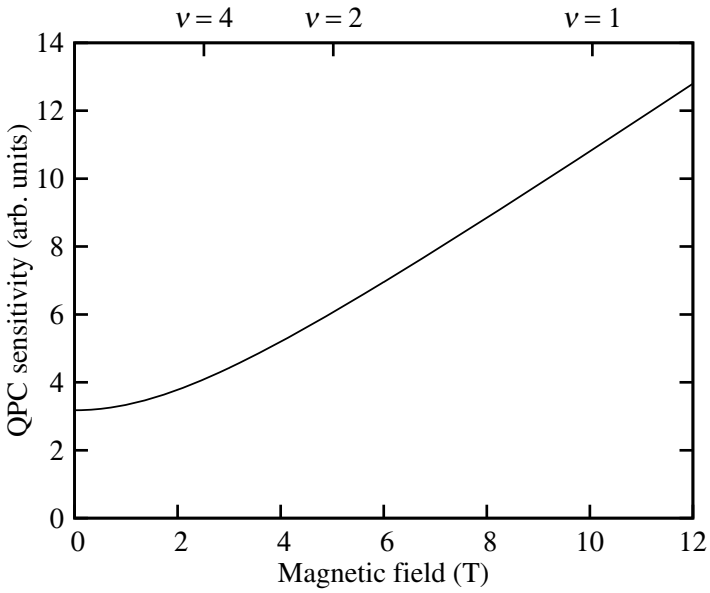

Figure 3. The relative sensitivity of the QPC, $\frac{1}{R}\frac{\mathrm{d}R}{\mathrm{d}E_\mathrm{F}}$, as a function of magnetic field. The sensitivity is inversely proportional to $E_1(B)$. The filling factors at which induced current features are observed are indicated along the top axis.

Induced currents cause a shift in the (quasi) Fermi energy, and $\Delta E = E_\mathrm{F} + \Delta E_\mathrm{F}$. From equation (1) the change in the Fermi energy causes a change in $R(B)$ of

$$\frac{\Delta R}{R(B)} = -\pi \frac{\Delta E_\mathrm{F}}{E_1(B)}. \tag{3}$$

Now the magnetic moment, Δm, produced by the induced currents may also be related to ΔE_F by the following argument [12]. For a circular sample of radius R the magnetic moment is related to the current density $J_\phi(r)$ by

$$\Delta m = \pi \int_0^R J_\phi(r) r^2 \,\mathrm{d}r = \pi \int_0^R \sigma_{xy} E_r(r) r^2 \,\mathrm{d}r, \tag{4}$$

where σ_{xy} is the Hall conductivity and $E_r(r)$ is the Hall electric field. Under the simplifying assumption of constant E_r, this reduces to $\Delta m = \sigma_{xy} E_r(r) \pi r^3/3$. The Hall electric field is caused by an accumulation of charge $e\Delta n$ per unit area at the edge of the sample (Δn is the change in 2D electron number density), and so $E_r = Ke\Delta n/\epsilon_0$ (K is a dimensionless numerical factor). However, Δn is related to the change in Fermi energy by $\Delta n = g(E_\mathrm{F})\Delta E_\mathrm{F}$, where $g(E_\mathrm{F})$ is the density of states at the Fermi energy. Thus

$$\Delta m = \frac{K\sigma_{xy}\pi r^3 e g(E_\mathrm{F})\Delta E_\mathrm{F}}{3\epsilon_0} \tag{5}$$

and hence

$$\Delta R = \frac{3\epsilon_0 R(B)}{K\sigma_{xy} r^3 e g(E_\mathrm{F}) E_1(B)} \Delta m. \tag{6}$$

We can use this equation to relate the filling-factor dependence of ΔR to that of Δm provided that we know the filling-factor dependences of all the quantities in the equation.

Table 1. Parameters used in the calculation of ΔR from Δm. The calculated value of ΔR assumes that $g(E_F)$ is independent of B.

Quantity	$\nu = 1$	$\nu = 2$	$\nu = 4$	Comments
Δm	1.7	1.7	1	Ratio, from figure 2
σ_{xy}	1	2	4	Ratio
$R(B)$	667 ± 10	231 ± 5	85 ± 0.5	Value, from figure 2
$E_1(B)$	0.37 ± 0.06	0.56 ± 0.03	1	Ratio, from figure 3
ΔR (calc.)	140 ± 20	16 ± 1	1	Ratio
ΔR (meas.)	72 ± 8	13 ± 2	1	Ratio, from figure 2

The filling-factor dependence of σ_{xy} is well known, that of $R(B)$ can be measured directly from figure 2 and that of $E_1(B)$ has been calculated above. Table 1 shows the parameters used in the calculation. Following the studies of Usher *et al* [13] and Zhu *et al* [14], whose magnetization measurements suggested the presence of a constant background density of states between Landau levels, $g(E_F)$ is assumed to be independent of field. However, the behaviour of $g(E_F)$ remains a matter of some controversy [1].

The magnetic-field dependences of the calculated and measured values of ΔR are in agreement at $\nu = 2$ and 4. The fact that the calculated value of ΔR at $\nu = 1$ is about twice as large as the measured value is probably due to the fact that the energy gap at $\nu = 1$ is a Zeeman gap and is therefore smaller than the gap at $\nu = 2$. This could lead to a larger $g(E_F)$ at $\nu = 1$ and hence a smaller value of ΔR than that calculated assuming constant $g(E_F)$.

3.2. Temperature dependence

Figure 4 shows the temperature dependence of the two measurements at $\nu = 1$ at a relatively high sweep rate of $3.2\,\mathrm{mT\,s^{-1}}$. The widths of the hysteretic features in both measurements reduce monotonically with increasing temperature, while the heights remain approximately constant up to a temperature of 400 mK and then gradually decrease as the temperature is increased further. For $\nu = 2$ (not shown) the magnetic moment and the QPC resistance again show similar temperature dependences, with the region of constant feature-height persisting up to 800 mK. At $\nu = 4$ the QPC resistance becomes too small to obtain a reliable temperature dependence. In figure 4, there is a significant difference, of about 0.15 T, in the magnetic fields at which the magnetic moment and resistance features occur, and there is a significant asymmetry to the resistance curves. This difference will be discussed below.

3.3. Sweep-rate dependence

Figure 5 shows the sweep-rate dependences of the magnetic moment and the hysteretic QPC resistance features at $\nu = 2$ and 4. These measurements can be thought of as current–voltage (I–V) curves for the induced currents: the sweep rate is proportional to the electromotive force around the perimeter of the 2DES, and the changes in magnetic moment or QPC resistance are proportional to the induced current. Both I–V curves show a saturation of the induced current at magnetic-field sweep rates greater than $\sim 0.5\,\mathrm{mT\,s^{-1}}$. This highly nonlinear behaviour is characteristic of the breakdown of the QHE at high currents [15]. For $\nu = 2$ (and $\nu = 1$,

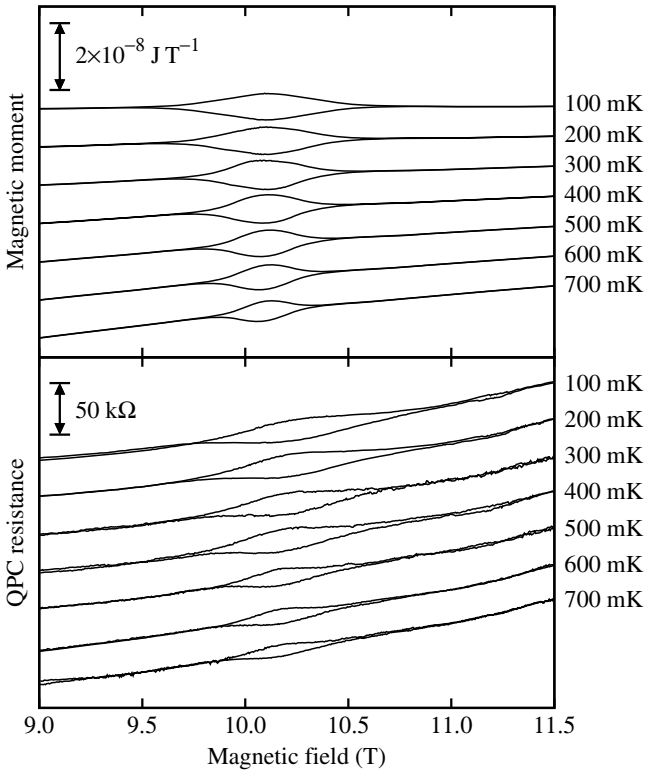

Figure 4. Temperature dependence of the induced current at $\nu = 1$ measured via its magnetic moment (top) and hysteretic QPC resistance (bottom). Both up- and down-sweeps are shown for each temperature, and each temperature is offset for clarity. The magnetic field was swept at a rate of $3.2\,\mathrm{mT\,s^{-1}}$. Features in both measurements are suppressed as the temperature is increased.

not shown), saturation occurs at the lowest sweep rate used in figure 5, $0.32\,\mathrm{mT\,s^{-1}}$, which corresponds to an electromotive force of 1.35 nV. This saturation is more marked than in the measurements of Pioro-Ladrière *et al* [8] probably due to differences in sample characteristics, but the underlying highly nonlinear behaviour is the same as those in this and other previous studies [15]. For $\nu = 4$, a more gradual reduction in the induced current is observed. In both cases, the shapes of the *I–V* curves derived from the two simultaneous measurements are the same within experimental error.

3.4. Noise

Figure 6 shows the induced current feature for $\nu = 2$ for both magnetic moment and QPC resistance using a very slow sweep rate of $80\,\mu\mathrm{T\,s^{-1}}$. Under these conditions previous investigators [16] observed a qualitatively reproducible 'noise' structure around the induced current peaks which they attributed to local QHE breakdown events occurring at various positions around the perimeter of the 2DES. In figure 6, several 'noise' features (e.g. those marked by arrows) appear in both measurements providing the strongest evidence to date that the two effects have a common cause. The fact that the noise features have similar sizes, relative to the $\nu = 2$ peaks, in both measurements lends support to the suggestion [5] that the induced current forms one loop around the entire 2DES, rather than many loops localized by impurities.

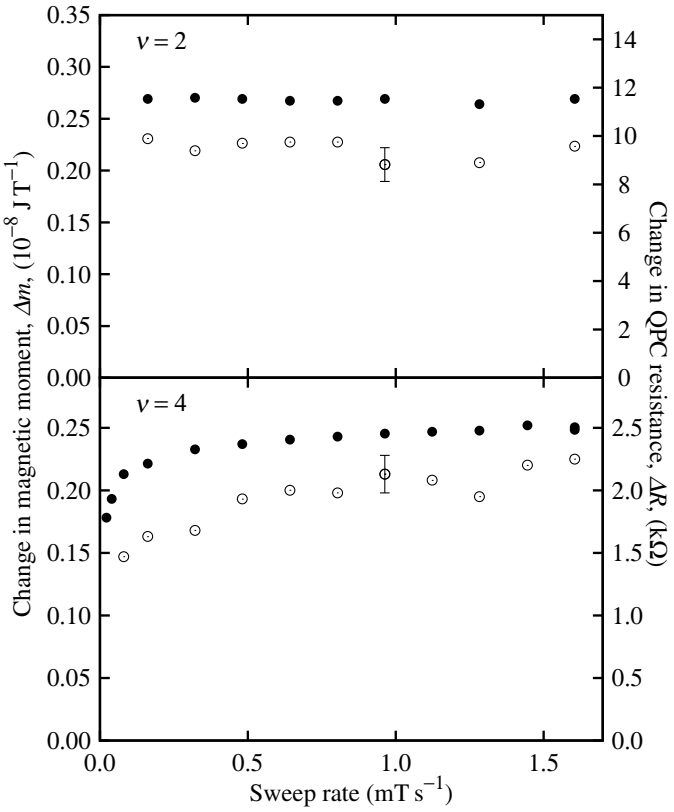

Figure 5. Sweep-rate dependences of the induced currents at $\nu = 2$ (top) and $\nu = 4$ (bottom) at 100 mK. The magnetic moment and QPC resistance were measured simultaneously. Filled symbols are magnetic moment and open symbols are QPC resistance. Typical error bars are shown for QPC resistance; for the magnetic moment, the error bars are of the same size as the symbols. The induced currents saturate at high sweep rates. At the slowest sweep rate accessible, the $\nu = 2$ induced current remained in the saturated regime.

Although the noise features occur at the same magnetic fields, the peaks of the induced current features (peak M in the magnetic moment and peak R in the QPC resistance) do not coincide, as noted earlier in section 3.2. The QPC resistance peak R is shifted to a higher magnetic field than the magnetic moment peak M, by about 0.021 T. Equation (6) shows that the QPC resistance has an extra magnetic-field dependence (through $R(B)$ and $E_1(B)$) compared with the magnetic moment, which would tend to shift the peak in QPC resistance to a higher field. However, this could not account for a shift of the observed magnitude. It is possible that this shift is also partly due to the background subtraction required in going from raw data (similar to that in figure 2) to the data of figure 6.

3.5. Decays

Figure 7 shows the decay of the induced current when the magnetic field is swept to filling factors $\nu = 1$ and 2 and then held constant, measured simultaneously from its magnetic moment and its effect on QPC resistance. The zeros of the decays are determined by sweeping in both

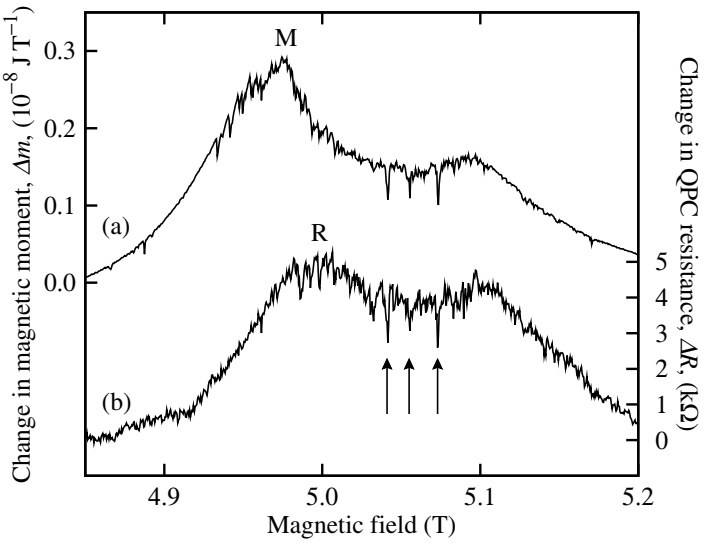

Figure 6. The induced current at $\nu = 2$, 100 mK, measured using a low sweep rate (80 μT s^{-1}). Arrows indicate three individual breakdown events which are correlated between the two types of simultaneous measurements, magnetic moment (upper trace) and QPC resistance (lower trace)—a clear demonstration that the two measurements share a common physical origin. The peaks labelled M and R are discussed in the text.

directions through the hysteretic features to determine a background level and then subtracting this background (for details of this procedure, see [17]).

At $\nu = 1$ both the magnetic moment and the QPC resistance show a rapid initial decay lasting approximately 20 s, followed by a much longer period of slower-than-exponential decay. This behaviour is consistent with the magnetic moment measurements of Kershaw *et al* [17] and is explained as follows: initially, the induced current is sufficient to cause breakdown of the QHE, and the resulting large dissipation causes a rapid decay; as the decay progresses, the current falls, the QHE recovers and the much lower dissipation drastically reduces the decay rate; in this regime the dissipation, and hence the decay rate, reduces gradually as the current decreases, resulting in a slower than exponential decay. The QPC resistance also appears to exhibit some drift in the opposite direction to the decay.

At $\nu = 2$ the magnetic moment decay behaves in the same way as at $\nu = 1$ (also consistent with [17]), but for the QPC resistance the slow-decay regime is replaced by a faster approximately linear decay. At $\nu = 4$ (not shown) the decay of both the magnetic moment and the QPC resistance is rapid and appears to be exponential. The trend towards faster decays at higher filling factors is due to the decrease in Landau-level separation, $\hbar\omega_c$ (where $\omega_c = eB/m^*$), as ν increases. We note here that although $\nu = 1$ is a spin-split feature (and hence the energy between the highest occupied and the lowest unoccupied Landau level is $g\mu_B B$, which is less than $\hbar\omega_c$), the process by which the decay occurs probably involves tunnelling, which one would expect to conserve spin—thus the levels involved in the tunnelling are separated by an energy $\hbar\omega_c$, not $g\mu_B B$. We attribute the difference in behaviour of the long-time decays at $\nu = 2$ to the sensitivity of the QPC resistance to the proximity of the induced current as well as its size—as the induced current decays, the Hall electric field supporting it is

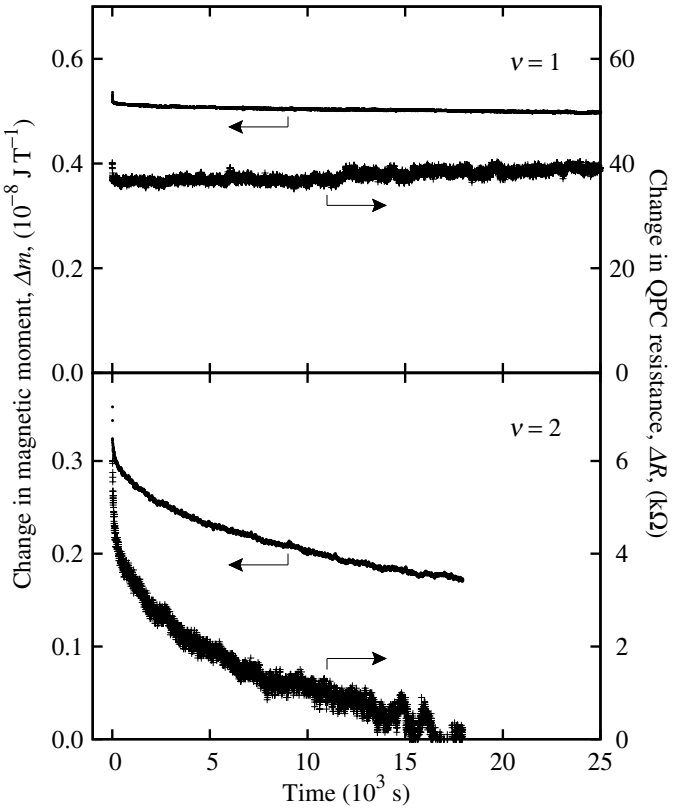

Figure 7. Simultaneous measurement of the decays of the induced current, (•) from magnetic moment and (+) from QPC resistance, at 100 mK. Top: at $\nu = 1$; bottom: at $\nu = 2$. The zeros of the decays are determined by sweeping through the induced current features in both directions, before and after the decay. A significant amount of drift, in the opposite direction to the decay, is evident in the QPC resistance at $\nu = 1$.

also reduced and the induced current becomes more spread out into the bulk of the 2DES. This effect is not apparent at $\nu = 1$ because the current does not decay sufficiently for spreading to become noticeable.

4. Conclusions

The observations discussed above show that induced currents cause hysteretic features in both the magnetic moment and the QPC resistance. We have also investigated the reverse effect, whether the QPC can be used to influence the induced current. For instance, during an induced-current decay, the bias on the QPC split gate was repeatedly changed to alternately pinch off the QPC and then open it to the point where the 2DES number density under the gate matched that in the bulk of the device. The expectation was that this would cause some extra dissipation and hence increase the decay rate. No such effect was observed. In another experiment, different voltages were applied to the two sides of the split gate, with the aim of setting up counter-propagating induced currents in close proximity, again with the expectation of enhanced dissipation. None was apparent. Further studies are necessary to determine how induced currents can be controlled by electrostatically defined nanostructures.

To conclude, in this paper we have demonstrated that the hysteretic features observed in the magnetoresistance of a QPC and the hysteretic features detected in the magnetic moment of the 2DES surrounding the device have a common origin—they are caused by long-lived induced currents which occur in the dissipationless regime of the QHE. We have shown this by carrying out simultaneous measurements of the two effects on the same QPC device, and correlating the features, their temperature and sweep-rate dependences, and their decays. We have also identified common features in the reproducible 'noise' structure observed at low sweep rates. It is clear that induced currents are responsible for both effects; however, a close comparison of the two measurements suggests that the hysteretic magnetoresistance of the QPC is sensitive not only to the size of the induced currents but also to their proximity to the QPC.

Acknowledgments

The authors thank K White for constructing the torsion-balance magnetometer and M Elliott and R J Nicholas for helpful discussions. This work was supported by EPSRC.

References

[1] Usher A and Elliott M 2009 *J. Phys.: Condens. Matter* **21** 103202
[2] Haavasoja T, Störmer H L, Bishop D J, Narayanamurti V, Gossard A C and Wiegmann W 1984 *Surf. Sci.* **142** 294–7
[3] Eisenstein J P, Störmer H L, Narayanamurti V and Gossard A C 1985 *Superlattices Microstruct.* **1** 11–4
[4] Jones C L, Usher A, Elliott M, Herrenden-Harker W G, Potts A, Shepherd R, Cheng T S and Foxon C T 1995 *Solid State Commun.* **95** 409–13
[5] Klaffs T, Krupenin V A, Weis J and Ahlers F J 2004 *Phys. E: Low-Dimens. Syst. Nanostruct.* **22** 737–40
[6] Chklovskii D B, Shklovskii B I and Glazman L I 1992 *Phys. Rev.* B **46** 4026–34
[7] Lier K and Gerhardts R R 1994 *Phys. Rev.* B **50** 7757–67
[8] Pioro-Ladrière M, Usher A, Sachrajda A S, Lapointe J, Gupta J, Wasilewski Z, Studenikin S and Elliott M 2006 *Phys. Rev.* B **73** 075309
[9] Fertig H A and Halperin B I 1987 *Phys. Rev.* B **36** 7969–76
[10] Matthews A J, Usher A and Williams C D H 2004 *Rev. Sci. Instrum.* **75** 2672–7
[11] Pioro-Ladrière M, Davies J H, Long A R, Sachrajda A S, Gaudreau L, Zawadzki P, Lapointe J, Gupta J, Wasilewski Z and Studenikin S 2005 *Phys. Rev.* B **72** 115331
[12] Kavokin K V, Portnoi M E, Matthews A J, Usher A, Gething J, Ritchie D A and Simmons M Y 2005 *Solid State Commun.* **134** 257–9
[13] Usher A, Zhu M, Matthews A J, Potts A, Elliott M, Herrenden-Harker W G, Ritchie D A and Simmons M Y 2004 *Phys. E: Low-Dimens. Syst. Nanostruct.* **22** 741–4
[14] Zhu M, Usher A, Matthews A J, Potts A, Elliott M, Herrenden-Harker W G, Ritchie D A and Simmons M Y 2003 *Phys. Rev.* B **67** 155329
[15] Jones C L, Usher A, Elliott M, Herrenden Harker W G, Potts A, Shepherd R, Cheng T S and Foxon C T 1996 *Solid State Commun.* **97** 763–8
[16] Elliott M, Lu Y, Phillips K L, Herrenden-Harker W G, Usher A, Matthews A J, Gething J D, Zhu M, Henini M and Ritchie D A 2006 *Europhys. Lett.* **75** 287–93
[17] Kershaw T J, Usher A, Sachrajda A S, Gupta J, Wasilewski Z R, Elliott M, Ritchie D A and Simmons M Y 2007 *New J. Phys.* **9** 71